Research Article

Dali Ramu Burada, Kamal K. Pant, Vinod Mishra, Mohamed Bichra, Gufran Sayeed Khan*, Stefan Sinzinger and Chandra Shakher

Development of a metrology technique suitable for *in situ* measurement and corrective manufacturing of freeform optics

https://doi.org/10.1515/aot-2018-0072
Received October 1, 2018; accepted April 23, 2019; previously published online May 23, 2019

Abstract: The applications of freeform optical surfaces in modern optical systems are providing unique solutions over rotationally symmetric surfaces. These surfaces offer higher degrees of freedom to the designer to enhance the high-end performance of the optical system. The precise metrology of freeform optics is one of the major bottlenecks for its use in imaging applications. Modern optical fabrication methods (i.e. fast or slow tool servo configuration) are, in principle, capable to meet the challenges to generate complex freeform surfaces if supported by precise metrology feedback for error compensation. In the present work, we have developed a Shack-Hartmann sensor-based metrology technique that can be used for quantitative *in situ* measurement of freeform optics. The sensor head is used to measure freeform optics in the reflection mode by following the CNC tool path in the offline mode. The measurements are used as feedback for corrective machining. Quantitative analysis is also performed to estimate the error budget of the metrology system. Further, the proposed *in situ* metrology scheme is validated by measuring freeform surface using a coherence correlation interferometric optical profiler.

Keywords: freeform optics; *in situ* measurement; scanning Shack-Hartmann sensor; subaperture stitching; ultra-precision machining.

***Corresponding author: Gufran Sayeed Khan,** Instrument Design Development Centre, Indian Institute of Technology Delhi, New Delhi 110016, India, e-mail: gufranskhan@iddc.iitd.ac.in. https://orcid.org/0000-0001-7911-565X
Dali Ramu Burada and Chandra Shakher: Instrument Design Development Centre, Indian Institute of Technology Delhi, New Delhi 110016, India
Kamal K. Pant: Instrument Design Development Centre, Indian Institute of Technology Delhi, New Delhi 110016, India; and Instruments Research and Development Establishment, Dehradun 248008, India
Vinod Mishra: Instrument Design Development Centre, Indian Institute of Technology Delhi, New Delhi 110016, India; and CSIR-Central Scientific Instruments Organisation, Chandigarh 160030, India
Mohamed Bichra and Stefan Sinzinger: Fachgebiet Technische Optik, Technische Universität Ilmenau, 98693 Ilmenau, Germany

1 Introduction

Freeform optical surfaces are nonrotationally symmetric surfaces that provide more degrees of freedom to the designer to minimize optical aberrations (i.e. astigmatism, coma, and distortion at multiple locations in the optical system) and make the system more compact by reducing size, weight, and volume [1–3]. The freeform surfaces are typically represented by extended polynomials [4], ϕ-polynomial [5], gradient-orthogonal Q-polynomials [6], nonuniform rational basis spline [7], radial basis functions [8], and Zernike polynomials [9]. These optical elements are found in nonimaging and imaging applications such as illuminations industries [10, 11], aerospace systems [12], biomedical engineering [13, 14], green energy [15], laser beam shaping [16], augmented reality [17, 18], and head-mounted display systems [19, 20]. Along with these advantages, there are numerous challenges involved in the design, manufacturing, and metrology of freeform surfaces. The present CNC-based ultra-precision manufacturing technologies are capable to fabricate such complex surfaces [21–23]. However, the performance of the manufacturing techniques are limited by the available metrology capabilities and a suitable feedback mechanism for an effective manufacturing process. To push the accuracy of the fabricated freeform surfaces, a measurement technique needs to be developed, which can measure the fabricated profile precisely on the machining platform, as an *in situ* measurement solution.

Coordinate measuring machine [24] can measure complex shapes, but the low-resolution data points can provide only the global shape of the freeform surface. A deflectometric technique [25] involves more computation to measure a freeform surface and also offers low-resolution measurement. Mechanical profiler [26], such as Form Talysurf, provides high-resolution measurement in a single scan. To record 3D shapes, an array of linear scans are required to be performed. Being contact in nature, such multiple linear scans destroy the surface. Optical profilers [27] are noncontact in nature and provide 3D shapes but have the slope limitations in single measurements. It is also a time-consuming process to scan the entire surface.

Interferometric techniques are typically used for rotationally symmetric surfaces, but by incorporating a null element in the setup it has been used for the measurement of freeform shapes also [28–30]. These null elements are surface specific and expensive to manufacture. QED Technologies (USA) developed non-null-based interferometric systems based on stitching principles with variable optical null elements to test mild aspheres; further, it has been extended to measure the shallow freeform optics [31]. Due to the complex setup and the requirement of vibration-insensitive platform, interferometric techniques, null or nonnull, cannot be used for *in situ* measurement. Tilted wave interferometry [32] has demonstrated the measurement capability of freeform optics. However, it is an offline measurement solution with limitations on the maximum slope that can be measured.

MarForm MFU200 (Mahr GmbH, Germany) [33] and LuphoScan (Taylor Hobson, UK) [34] are point-based sensors where the optical probe can be placed normal to the surface by means of two linear and one rotary stages. The sensor can measure rotationally symmetric surfaces with high accuracy. In principle, they can also be used for the measurement of freeform shapes, but the measurement uncertainties are larger for the measurement of high slope freeforms. Recently, a noncontact point cloud metrology technique based on swept source optical coherence tomography is developed for the measurement of freeform optics. It is coupled with an interferometric system having multiple scanning stages. It is demonstrated to measure the freeform surfaces in 1-inch diameter class and up to 10° in slope [35].

All the methods and the instruments discussed above measure the optical elements in offline mode. Due to the nonrotational symmetric nature of the freeform profiles, the offline measurement requires precise mounting and demounting of the surface part, failing that causes indexing errors. Shack-Hartmann sensors (SHS) have the potential to be integrated into the machining platforms due to its low vibration sensitivity, compactness, and simple principle of operation for the measurement of form errors. A typical SHS can measure large slope, of the order of 25°, depending on the diameter, focal length, and the number of lenslets in the array. We reported a scanning subaperture stitching scheme for measurement of freeform wavefronts using SHS as slope measurement sensor [36–38]. The scheme has been used for the measurement of freeform surface in transmission mode. However, to be able to measure the profile of the freeform surface *in situ* and to provide the metrology feedback to the machining platform for corrective machining cycles, a measurement in reflection mode is required. We have recently described a scheme for the measurement of freeform optics in reflection mode as shown in Figure 1 [39]. The collimated beam after reflection from a beam splitter interacts with the surface under test. The reflected wavefront from the freeform surface is diverging in nature, and it carries the information about the surface shape that is measured at the detector plane using a scanning SHS. The lateral extent of the wavefront is larger in size than the detector size of the SHS head. Hence, multiple subapertures are required to be measured by scanning the SHS along the X and Y directions to cover the entire wavefront. Finally, all the subapertures are stitched together using a stitching algorithm developed in-house [36, 38]. Our first implementation of the scheme has been successfully demonstrated within the limits of the manual positioning of the SHS during scanning. Simulation studies to understand the effects of misalignments on the measurement accuracy have been presented.

The scheme has limitations on the maximum slope that can be measured and we could only measure a small area (~3 mm) of a freeform with shallow slope. The dynamic range of the SHS limits the maximum slope that could be measured in a subaperture. In this paper, we present an improved measurement scheme that can

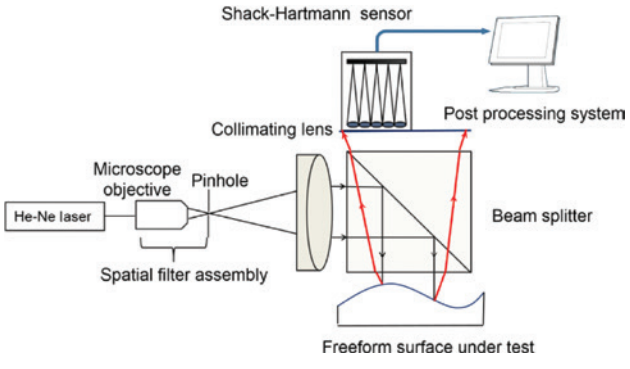

Figure 1: Basic principle of operation of the scanning SHS-based measurement in reflection mode.

measure steep freeform surfaces with large aperture size. The size that can be measured is basically limited by the scanning stages used during the measurement. It can easily be incorporated in the machine head using its computer-controlled translation, tip-tilt, and rotational axes. The scheme is better suited for efficient correction of the tool path to compensate the form error. The capability of the scheme has been demonstrated by measuring the form error of a steep freeform surface. The measurements have been further used as a feedback for the correction of the tool path for form error compensation.

2 Measurement setup

Instead of placing the scanning SHS normal to the freeform wavefront, as described in Ref. [39] and shown in Figure 1, we chose a setup shown in Figure 2, where the SHS is placed normal to each subaperture of the wavefront. The SHS is mounted on six-axes precise computer-controlled scanning stages (tip, tilt, rotational, and three translational), which make it capable to scan the wavefront in a manner shown in Figure 2. The advantage of this configuration is that the maximum slope to be measured in each subaperture is reduced. This in turn enhances the capability to measure steep surfaces as it becomes possible to place the SHS head normal to each subaperture by following the geometry of the freeform surface. The technique offers the flexibility to measure large freeform surface/wavefront areas. Further, this configuration can be used as *in situ* measurement of freeform surface by integrating it into machining platform.

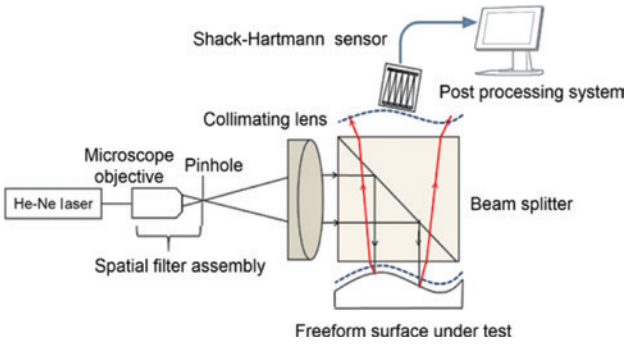

Figure 2: Scanning SHS normal to each subaperture of freeform wavefront.

2.1 Alignment and calibration process

The calibration process of the setup is performed by measuring a reference optical flat before performing the measurement of freeform optics. Before the measurement, a prealignment of the SHS sensor is done to adjust its orientation to ensure the orthogonality of the SHS with respect to the incident collimated beam. Larger tilt in the incident beam needs to be avoided, which otherwise does not provide good measurement conditions and causes higher measurement uncertainty. The process uses a prealigned reference flat in the reflection mode with an alignment ring. The alignment ring is a circular plate with a central hole of diameter 0.5 mm mounted in front of the SHS. This allows only a small portion of the light beam to enter the SHS assembly and forms small spot patterns on the detector. The spot patterns are adjusted to fall inside a software-generated circular pattern to ensure the minimal tilt as shown in Figure 3. Once this prealignment is done, the reference optical flat is replaced by the freeform optics under test. As freeform surface has nonrotational symmetric nature, the alignment of both the surface and the SHS is a challenging task. Therefore, an iterative alignment process is developed for the SHS suitable for the measurement of freeform surface. In this process, SHS is aligned to the center portion of the freeform surface until the residual error is as minimum as possible compared to

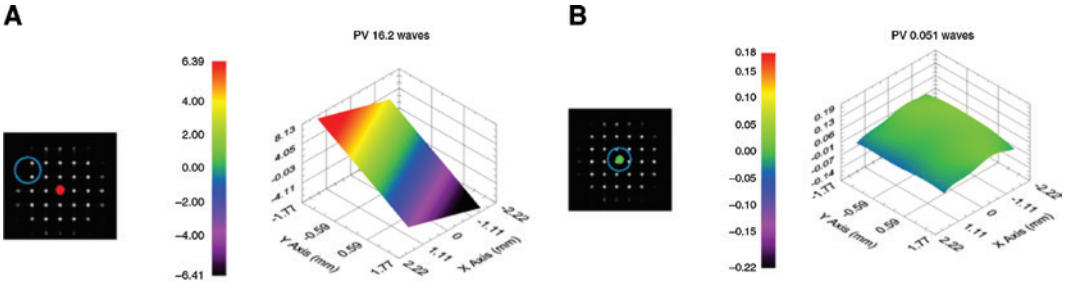

Figure 3: Alignment/calibration process of the SHS: (A) spot diagram and plane wavefront when SHS is misaligned and (B) spot diagram and plane wavefront after the SHS is aligned.

its geometrical surface part. Further, SHS is aligned to the two extreme corner subapertures of the surface. Thereafter, it is assumed that the SHS will remain aligned normal to the each subaperture during measurement.

2.2 Freeform wavefront reconstruction scheme

The measurement of freeform wavefront is performed by scanning the entire surface to measure all the subapertures with consistent overlapping area. Using in-house stitching software, the misalignments are corrected and subapertures are stitched to give the phase profile of the entire freeform wavefront. The size of the beam splitter is an important parameter that is required to be prudently selected based on both the divergence of the reflected beam and the slope of the freeform surface. In the case of a small beam splitter size and a steep diverging reflected wavefront, the beam splitter will itself be a limiting aperture and restricts the size of the freeform surface to be measured [39]. A beam splitter of diameter 12.7 mm has been used in the experiment. It is assumed that any optical aberration induced due to the insertion of the beam splitter is very less and does not affect the measurement.

A freeform surface of phase profile shown in Figure 4A is chosen as specimen under test. It is described by a seventh-order polynomial. It is made up of polymethyl methacrylate (PMMA) with the physical dimensions of 14 × 14 mm and the maximum sag of 1.119 mm. It can be represented by the sag equation as

$$z = \frac{c(x^2+y^2)}{1+\sqrt{1-(1+k)c^2(x^2+y^2)}} + \sum_{i=1}^{N}\sum_{j=1}^{N-i} A_i(N)x^{i-1}y^{j-1}$$

Here, the first term represents the conic section, where c is the curvature, x and y are the Cartesian coordinates, and k is the conic constant. The second term represents the Nth order polynomial with x and y sample points. A_i are the polynomial coefficients. In this study, the first term of the sag equations is taken as zero and the second term is the seventh-order polynomial. The vertex point of the phase profile is shifted by 1 mm and 1.3 mm in the X and Y directions, respectively, from the geometrical center of the wavefront. In this study, an SHS from Imagine Optic (France) is used. The dynamic range of the SHS is 0.85° (15 mrad) per lenslet. The detailed specifications of both the test specimen and the SHS are given in Table 1.

The scanning SHS head needs to follow the profile of the freeform wavefront as shown in Figure 2. The position coordinates and tilts in X and Y directions for each subaperture need to be calculated first. Table 2 presents the required position coordinates and tilts of the SHS for each subaperture for the freeform surface under test. The wavefront is divided into 5 × 5, i.e. 25 subapertures.

Simulation studies are first performed to estimate the reconstruction error of freeform wavefront from its calculated slope data before conducting the experiment. The wavefront at 34 mm distance from the vertex of the freeform is measured. It is due to the minimum possible physical distance between the freeform surface and the lenslet array of SHS head in the actual experimental setup. First, the full wavefront at 34 mm distance is calculated through ray trace. The full wavefront is of the size 11.27 × 11.27 mm², which represents 6.27 × 6.27 mm² actual area on the surface part. The peak-to-valley (PV) of the freeform wavefront at the propagated distance is 989.8 waves (1 wave = 632.8 nm) as shown in Figure 4B. The maximum slope of the measured wavefront along X and Y directions is 0.98° (17.24 mrad) and 0.68° (12.03 mrad), respectively.

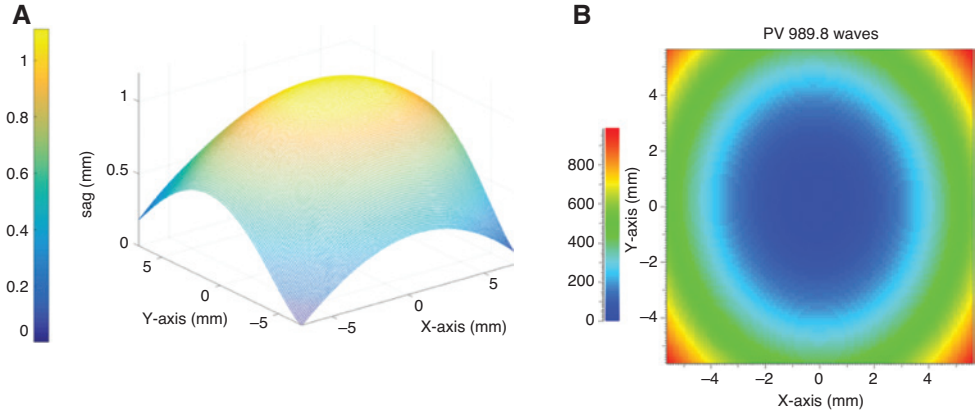

Figure 4: (A) Freeform profile under test and (B) propagated freeform wavefront map at 34 mm distance from the surface (PV 989.8 waves, 1 wave = 632 nm).

Table 1: Freeform surface and SHS specifications.

Surface under test		Scanning wavefront senor	
Surface type	Cubic phase plate	Microlens aperture size	$114\times114\ \mu m^2$
Material	PMMA	Focal length	3.8 mm
Profile	Seventh order polynomial	Microlens array size	$4.56\times3.56\ mm^2$
Maximum sag	1.11 mm over $14\times14\ mm^2$	Total number of lenses in the array	40×32
	0.376 mm over $6.27\times6.27\ mm^2$		
Maximum slopes	Surface slope over $14\times14\ mm^2$	Pixel size of CCD	$6.7\times6.7\ \mu m^2$
	X slope: 0.80° (14.09 mrad)		
	Y slope: 0.68° (11.88 mrad)		
	Surface slope over $6.27\times6.27\ mm^2$	Dynamic range of SHS	0.85° (15 mrad)
	X slope: 0.64° (11.17 mrad)		
	Y slope: 0.38° (6.63 mrad)		

Table 2: SHS metrology head position coordinates and tilts required for measurement of each subaperture.

Subaperture	Position (mm)		Angle (tilt, °)		Subaperture	Position (mm)		Angle (tilt, °)	
	X	*Y*	θ*x*	θ*y*		*X*	*Y*	θ*x*	θ*y*
1	−3.14	−2.84	0.3438	−0.06047	14	3.07	1.3	−0.003456	0.3454
2	−1.07	−2.84	0.3551	−0.3322	15	5.14	1.3	−0.01515	0.6325
3	1	−2.84	0.4008	−0.001066	16	−3.14	3.37	−0.2121	−0.6522
4	3.07	−2.84	0.3554	0.3302	17	−1.07	3.37	−0.2001	−0.3567
5	5.14	−2.84	0.3442	0.6017	18	1	3.37	−0.1955	−0.001418
6	−3.14	−0.77	0.1725	−0.6199	19	3.07	3.37	−0.1998	0.354
7	−1.07	−0.77	0.1837	−0.3396	20	5.14	3.37	−0.2116	0.6485
8	1	−0.77	0.1877	−0.001194	21	−3.14	5.44	−0.4087	−0.6667
9	3.07	−0.77	0.184	0.3454	22	−1.07	5.44	−0.3977	−0.365
10	5.14	−0.77	0.1729	0.6167	23	1	5.44	−0.3934	−0.001519
11	−3.14	1.3	−0.01551	−0.636	24	3.07	5.44	−0.3971	0.3621
12	−1.07	1.3	−0.003678	−0.3467	25	5.14	5.44	−0.4082	0.6626
13	1	1.3	−0.0007039	−0.001306					

It is the wavefront that needs to be measured using subaperture stitching scheme.

The reconstruction of the freeform wavefront has been performed in an ideal situation, i.e. no misalignments between adjacent subapertures using RAYTRACE software [40]. The full measured wavefront is divided into 5×5 subapertures as shown in Figure 5A and B. The size of the individual subapertures is $2.99\times2.99\ mm^2$ and the overlapping area of 30% has been maintained between the adjacent subapertures. The scanning SHS head follows the profile of the freeform surface, as shown in Figure 2, with prior calculated position coordinates and tilts in *X* and *Y* directions for each subaperture as shown in Table 2.

The scanned subaperture slope data have been reconstructed based on a weighted cubic spline integration method [38] and then stitched using in-house developed subaperture stitching algorithm [36]. A subaperture stitching algorithm minimizes the misalignments between adjacent subapertures based on the least-squares fitting method. The misalignments in the vertical plane, i.e. piston, tilt, and power, are minimized by fitting them in the overlapping zone. An iterative alignment is used to minimize the radial and rotational misalignment errors during registration in global frame before the stitching process as mentioned in Section 2.1. Once the misalignments are minimized, a data averaging method is used to connect the phase profile of the registered subapertures to obtain a full wavefront map and it has 989.79 waves of PV (Figure 5C). It is compared to its nominal profile shown in Figure 4B. Figure 5D is the residual wavefront map with PV of 0.005 waves and RMS of 0.00044 waves without any misalignment. The negligible error in the residual wavefront map shows the accuracy of the stitching process when there are no misalignments/registration error in the subapertures.

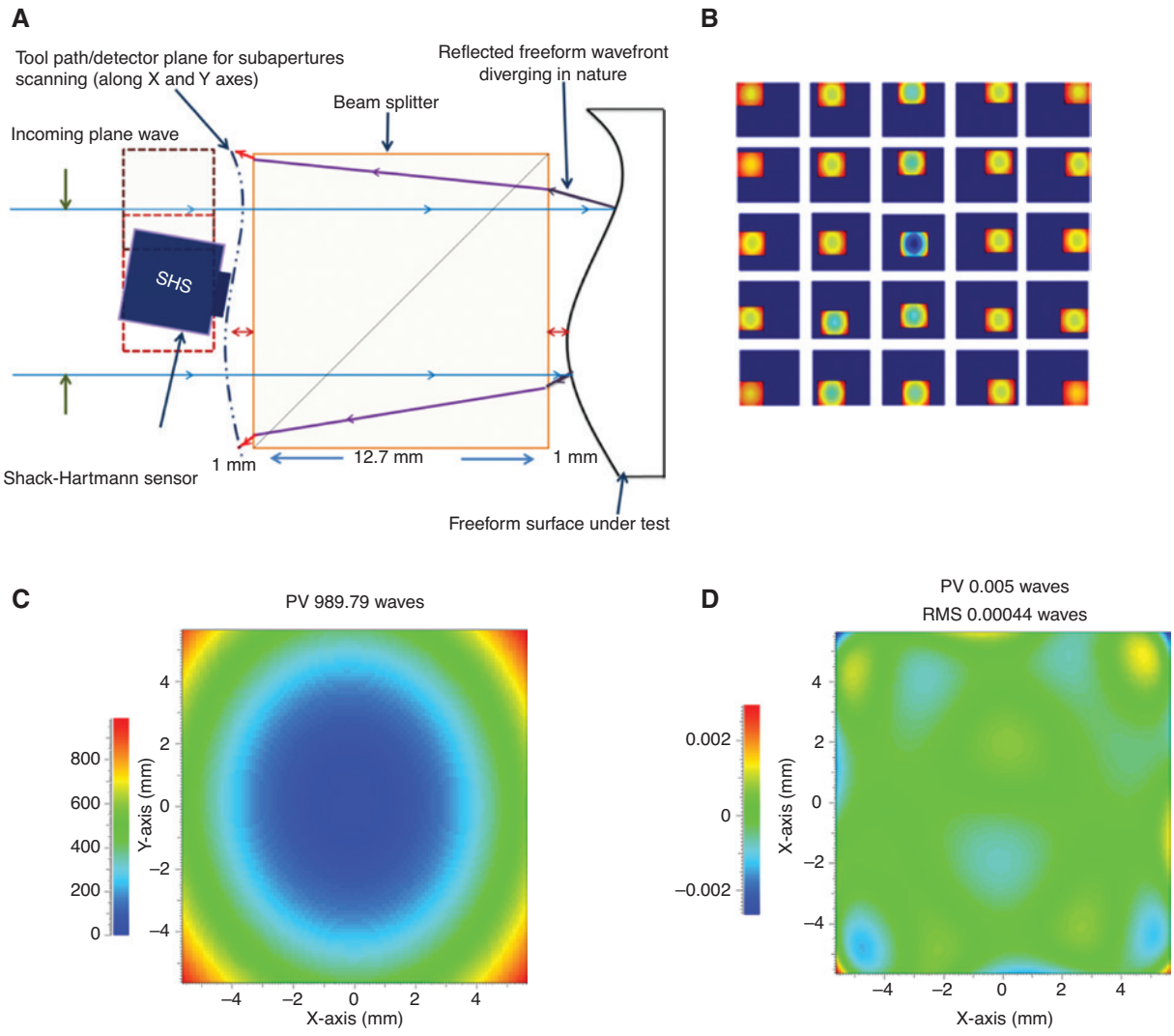

Figure 5: (A) Raytracing method to simulate subapertures, (B) 5×5 subapertures, (C) stitched wavefront map in the ideal situation (PV 989.79 waves), and (D) residual wavefront in ideal situation (PV 0.005 waves, RMS 0.00044 waves).

3 Experimental results

3.1 SHS head-based metrology for freeform wavefront

The freeform profile is fabricated in PMMA using a five-axes ultra-precise machining platform (Nanoform 200) in slow tool servo configuration. Figure 6 shows the experimental setup that has been developed for the measurement of freeform surface/wavefront. The measurement of the fabricated profile is performed as per the procedure described in Section 2. An He-Ne laser source ($\lambda = 632.8$ nm) is used in the experiment. The area of the surface (6.27×6.27 mm^2) keeping vertex point at the center has been illuminated and the divergent wavefront at a distance of 34 mm (i.e. at the detector plane) is measured. The measurements are taken as per the scheme in Section 2.2.

All the subapertures are aligned individually relative to their nominal positions (as calculated and presented in Table 2) before taking the measurements. Figure 7A shows the 25 experimentally measured subapertures. The scanned subapertures are stitched to obtain a full wavefront map. Figure 7B shows the wavefront map that exhibits a PV deviation of 986.54 waves. A point-to-point comparison has been done with the ideal freeform wavefront propagated to a distance of 34 mm (Figure 4B). The residual wavefront error is 18.4 waves of PV as shown is Figure 8.

3.2 Modeling of freeform surface profile from the measured wavefront

The experimentally stitched wavefront (Figure 7B) is back-propagated by performing the reverse raytracing as shown in Figure 9A. The following are the steps for the calculation of the surface profile under test from the experimentally measured wavefront:

(a) An optical surface is simulated from the measured wavefront and placed at the same position where the wavefront is measured.

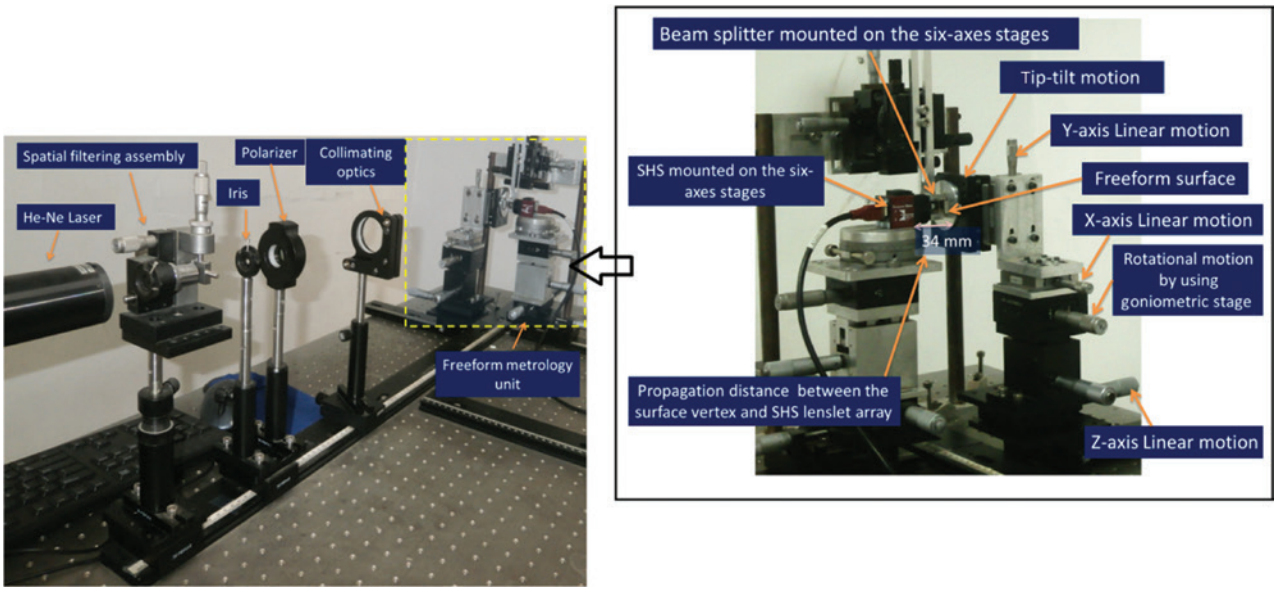

Figure 6: Experimental setup for the measurement of freeform optics. The inset shows a multiaxis mounting assembly unit of the freeform surface under test, beam splitter, and SHS.

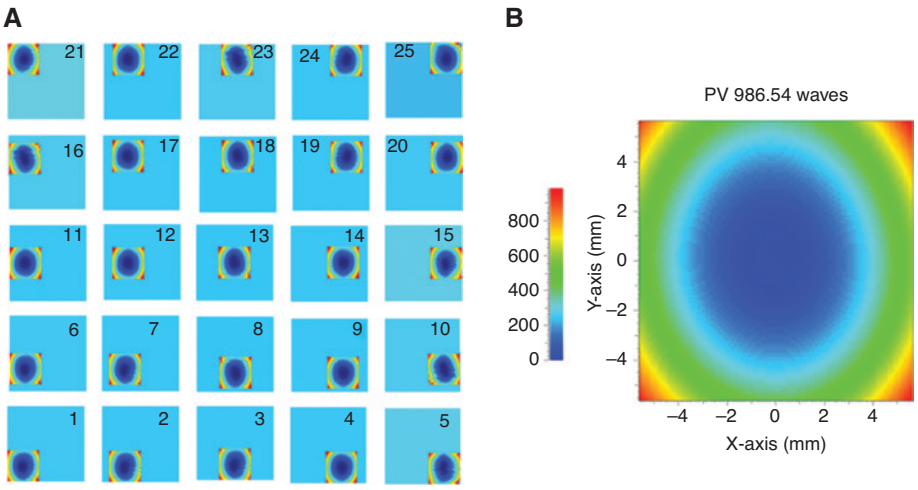

Figure 7: (A) Experimental measured subapertures and (B) experimental stitched wavefront (PV 986.54 waves).

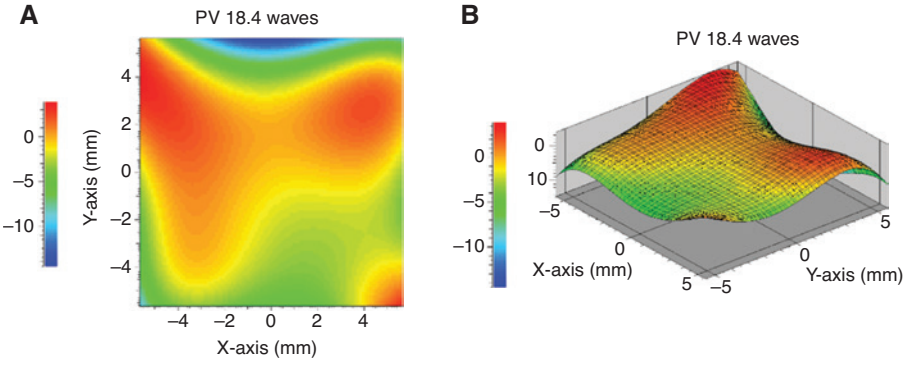

Figure 8: (A) Residual wavefront error map of experimental stitched wavefront to ideal wavefront and (B) 3D map of residual profile (PV 18.4 waves).

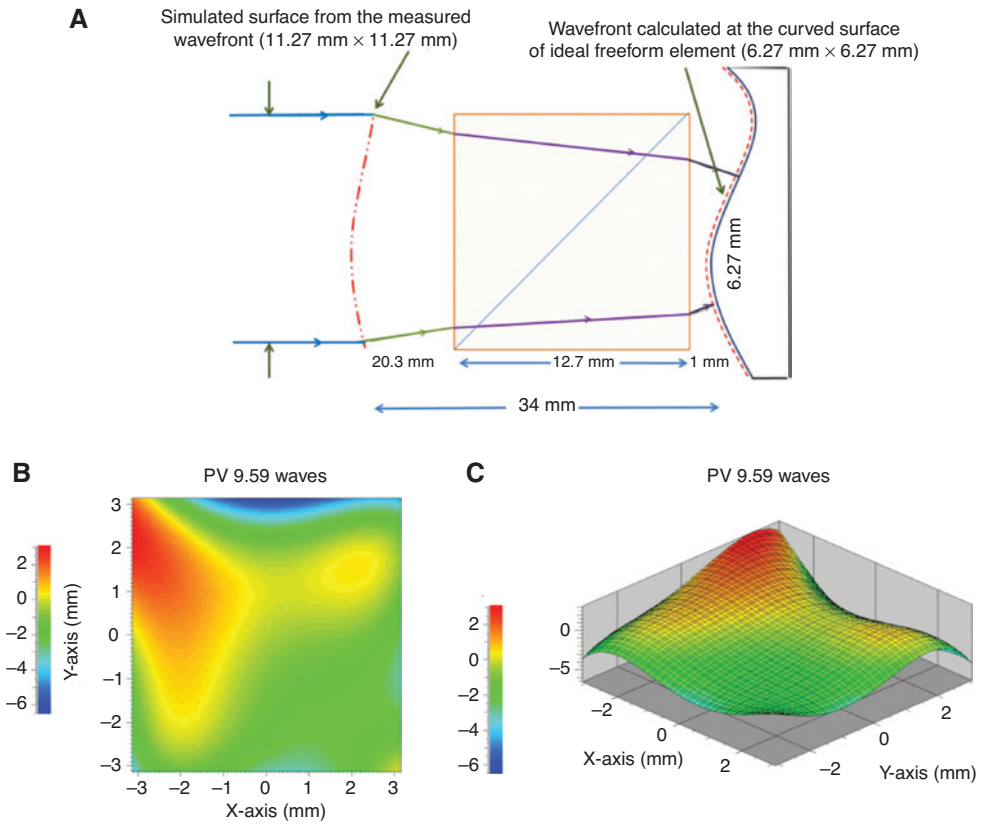

Figure 9: (A) Geometric raytracing scheme for back-propagation of the measured freeform wavefront, (B) profile error on the freeform surface, and (C) profile error in 3D (PV 9.59 waves).

(b) A grid of collimated rays perpendicularly emitting from the simulated surface are traced back to the curved profile of the ideal freeform element using the RAYTRACE software [40]. The parallel rays coming from the left side are just auxiliary rays due to the software implementation and determine the starting points on the simulated freeform surface where the rays are now perpendicular to the simulated freeform surface and have all phase zero.

(c) The wavefront is calculated at the curved profile of the ideal freeform surface under test placed at the same distance as in the actual experiment. At this distance, the back-propagated freeform wavefront represents the surface part that has been measured.

(d) The simulated surface from the back-propagated freeform wavefront is then compared to the ideal geometrical surface. The residual profile error (shape errors) is obtained by taking a point-to-point difference.

The derived shape error on the freeform surface of PV deviation of 9.59 waves is shown in Figure 9B and C.

3.3 Feedback mechanism for corrective machining

The residual surface error map (Figure 9B) is used to compensate the tool path in the corrective CNC machining process. The data of residual surface error map are fed into the machine tool path using the format compatible to the machining platform, i.e. the polar coordinate system. The error map has been rearranged into the polar coordinate system to modify the tool path in a point-by-point configuration. The modified tool path is used for the corrective machining to reduce the profile error. The machined surface has been measured and the residual surface error after tool path compensation is of 3.60 waves of PV as shown in Figure 10. A significant improvement is achieved using feedback from the SHS metrology method. The above tool path compensation process proved the capability of SHS-based method for *in situ* metrology and feedback for form error correction. The only drawback is the limited number of data points and the resolution offered by the SHS (Table 1). However, when used *in situ*, it can provide fast convergence toward achieving the desired shape through error feedback mechanism.

3.4 Repeatability and reproducibility tests

Repeatability and reproducibility tests are conducted to validate the performance of the developed scheme. Repeatability is the difference between the two consecutive measurements without any change in the system. It yields the facts about the sensitivity of the experimental setup, such as vibration, temperature, and other sensor noise. Twenty such repeatability measurements at the time interval of 30 s each are performed. Figure 11A shows the average of the 20 repeatability results of subaperture measurements. The PV is 0.012 waves and the RMS is 0.0018 waves.

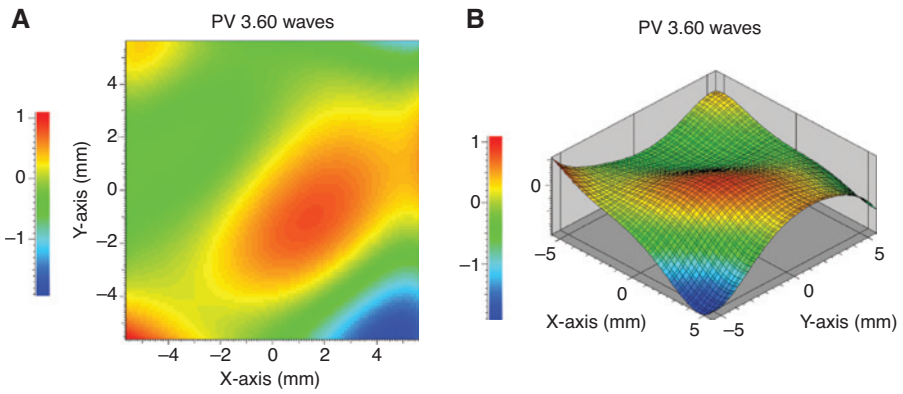

Figure 10: (A) Shape error of the freeform surface after tool path compensation and (B) 3D map of residual profile (PV 3.60 waves).

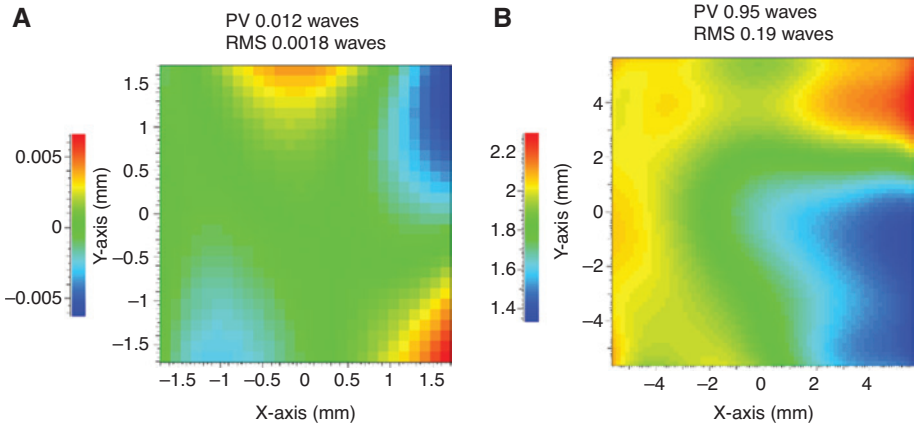

Figure 11: (A) Repeatability of the single subaperture measurement (PV 0.012 waves, RMS 0.0018 waves) and (B) reproducibility of the stitched wavefront map (PV 0.95 waves, RMS 0.19 waves).

As the measurement scheme requires movements of SHS to scan the complete wavefront, it is important to understand the effects of positioning errors during the scanning process. It has been captured by performing reproducibility test. The measurement of the entire wavefront shown in Section 3.1 (Figure 7B) has been repeated five times. The average reproducibility of the measurements is shown in Figure 11B. The PV is 0.95 waves and the RMS is 0.19 waves. It is also observed that the reproducibility depends on the slope of the wavefront to be measured. The lesser the slope to be measured, the better is the achievable reproducibility.

4 Quantitative analysis: simulations

To understand the uncertainties involved in the measurement scheme, a quantitative analysis has been carried out. The influence of misalignment and the overlapping area of subapertures on stitching accuracy have been investigated by performing simulations.

4.1 Influence of lateral and rotational misalignments on stitching accuracy

In practical situation, the lateral (i.e. translational and rotational errors) and vertical (i.e. piston, tip-tilt, and defocus) misalignments may present due to the scanning stages of the SHS. These misalignments of the subapertures will limit the stitching accuracy. The vertical misalignments are corrected using the least-squares fitting algorithm. The lateral misalignments correction is, however, more challenging to address for achieving better stitching accuracy. To estimate the influence of the lateral misalignments, a study has been conducted by introducing various misalignments in the 5×5 subapertures array. The misaligned subapertures have been stitched and compared to the ideal wavefront. The resulted residual error represents the stitching accuracy in this investigation.

Table 3 presents the residual error when the subapertures have been misaligned by 10 μm in X and Y

Table 3: Stitching error budget analysis before alignment of the freeform surface.

Case	Translations error (μm)			Angular rotational error (°)	Angular tilt error (°)	Stitching error (residual) (waves)	
	Tx	Ty	Tz	Φ	θ*xy*	PV	RMS
1	−10	0	0	0	0	0.29	0.004
2	0	10	0	0	0	0.14	0.0023
3	0	0	−10	0	0	0.44	0.090
4	0	0	0	0.5	0	10.29	1.62
5	0	0	0	0	0.5	6.23	0.92
6	−10	10	−10	0.5	0.5	19.13	3.38

directions and rotated by 0.5°. The translational and rotational stages used in the experiment have the resolution of 1 μm and the 0.017° (1 arc min), respectively. The reconstructed stitching accuracy has been estimated by introducing the misalignments within resolution of the stages, and Table 4 presents the stitching error budget. It is observed that the rotational misalignments (case 4 in Table 4) are more critical than the translational misalignments. Case 6 represents a simulated situation when all the translation stages have 1 μm misalignment error and all rotational stages have 0.017°. The observed stitching error is 0.64 waves. This represents the estimated highest stitching error with the used scanning stages assuming that the positioning accuracy is within 1 μm. However, any error in the straightness of the mechanical mount/assembly may lead to larger positioning inaccuracies and needs special attention during mounting.

To know the effects of internal sensor error on the measurement as well as stitching process, a collimated wavefront of diameter 6.27 × 6.27 mm² has been measured using the scanning stitching scheme. The total of nine subapertures of the same size (i.e. 2.99 × 2.99 mm²) are measured and stitched together. The overall wavefront deviation is 0.15 waves. This shows that the systematic error of the scanning SHS on the measurement is quite small.

Table 4: Stitching error budget analysis after alignment of the freeform surface.

Case	Translations error (μm)			Angular rotational error (°)	Angular tilt error (°)	Stitching error (residual) (waves)	
	Tx	Ty	Tz	Φ	θ*xy*	PV	RMS
1	−1	0	0	0	0	0.04	0.0068
2	0	1	0	0	0	0.02	0.0040
3	0	0	−1	0	0	0.08	0.019
4	0	0	0	0.017	0	0.35	0.052
5	0	0	0	0	0.017	0.021	0.030
6	−1	1	−1	0.017	0.017	0.64	0.011

4.2 Influence of overlapping area on stitching accuracy

A consistent overlapping area is required between adjacent subapertures to minimize the effects of misalignments and provides an optimal performance of stitching process. A smaller overlapping area causes larger stitching errors, whereas a larger overlapping area results more number of subapertures and leads to longer computational/measurement time. To know the influence of the overlapping area on the stitching accuracy quantitatively, a study has been conducted by varying the overlapping area between the adjacent subapertures from 10% to 50%. The subapertures have been misaligned by the amount within the resolution of the scanning stages used as discussed in Section 4.1. The subapertures with the individual size of 2.99 × 2.99 mm² (i.e. 28 × 28 sample points) are simulated for different overlapping areas and stitched to obtain a full wavefront map. The reconstructed stitched wavefront map is compared to the respective ideal wavefront maps. The residual errors are gradually decreasing with the increase of the overlapping area as shown in Figure 12. It is evident that the overlapping area more than 30% does not significantly increase the stitching accuracy further.

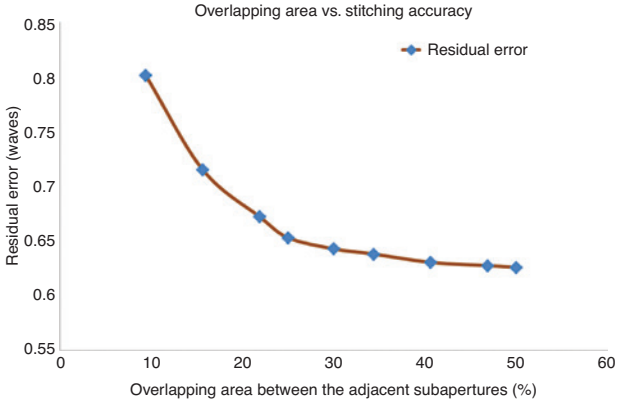

Figure 12: Influence of the overlapping area on the subaperture stitching.

5 Validation of the SHS-based metrology using coherence correlation interferometric optical profiler

Due to the nonavailability of a standard metrology technique for freeform optics until date, the validation of the developed SHS metrology method is quite challenging. For the validation purpose, a coherence correlation interferometric optical profiler has been chosen for the metrology of freeform optics. However, the optical profilometric techniques have limitations on the maximum sag, which can be measured. The freeform surface measured in the previous section is having steep sag and hence could not be measured using the available optical profiler (Talysurf CCI 6000, Taylor Hobson make). Therefore, a freeform surface with low slopes has been fabricated and tested by the coherence correlation interferometric optical profiler and the developed scanning SHS technique. The profile of the surface has been scaled down where the slopes along X and Y directions are 0.063° (1.1 mrad) and 0.08° (1.4 mrad), respectively, and the sag of 0.111 mm over 14×14 mm^2 area. The phase profile of the measured full freeform wavefront at a propagated distance of 34 mm has the maximum slopes along X and Y directions are 0.118° (2.05 mrad) and 0.069° (1.20 mrad), respectively.

The freeform wavefront has been measured at a distance of 34 mm by taking 3×3 subapertures over the area of 7.752×7.752 mm^2. The actual area represented on the surface is 6.8×6.8 mm^2. The size of the individual subapertures is 3.192×3.192 mm^2 with the overlapping area of 28% between the adjacent subapertures. The experimentally stitched wavefront has been back-propagated at the surface and compared to the nominal profile. The residual error is 7.8 waves of PV as shown in Figure 13. The same surface has been measured using optical profiler (Talysurf CCI 6000). Figure 14 shows the surface profile map of the freeform optics measured by CCI. The PV of the surface error is 7.92 waves.

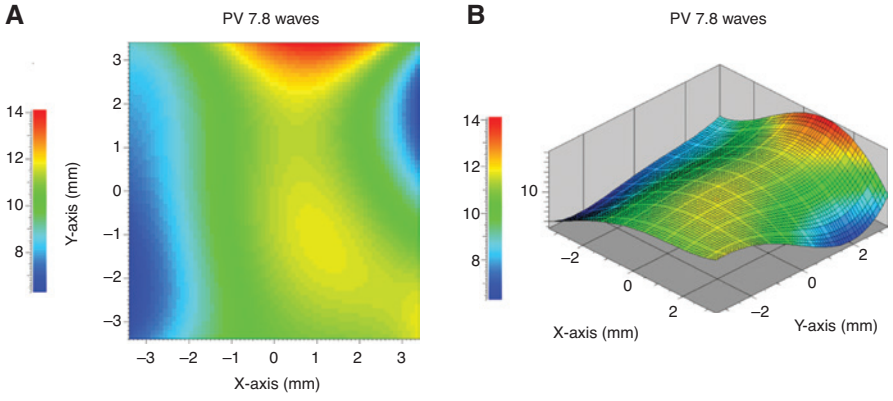

Figure 13: Surface profile measurement using a scanning SHS: (A) shape error on the freeform surface (PV 7.8 waves) and (B) 3D map of shape error (PV 7.8 waves).

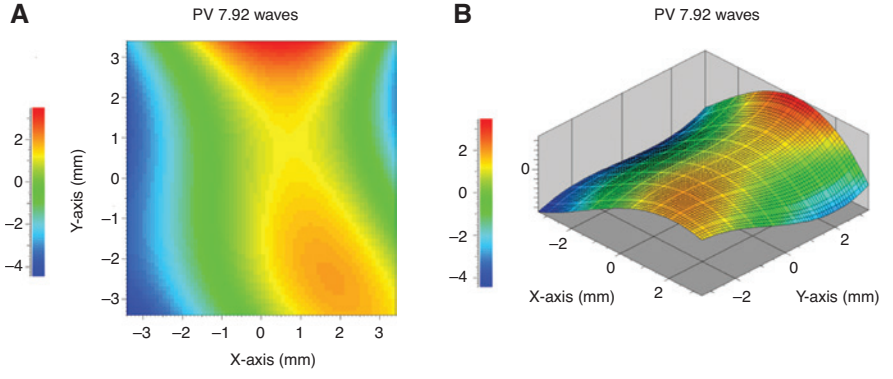

Figure 14: Surface profile measurement using a coherence correlation interferometric optical profiler: (A) shape error on the freeform surface (PV 7.92 waves) and (B) 3D map of shape error (PV 7.92 waves).

Both measurement techniques, SHS and optical profiler, are performed in reflection mode. Although both measurement schemes and measurement principles are different, the results are in good agreement. One can observe that the global error shape is quite similar in both measurements. This comparative study validates the metrology scheme developed under this research work.

6 Conclusions

In this paper, we introduce a subaperture measurement technique for freeform optics using a scanning SHS head in reflection mode. The fabrication of freeform surface is done by slow tool servo configuration of ultra-precision machining. The wavefront reflected from the freeform surface under test has been measured by capturing subapertures while moving the scanning SHS head normal to the freeform wavefront. The measured wavefront has been back-propagated to obtain the profile error. The residual profile error map is used as an input for the tool path compensation for form error correction. The measured profile error on the component after tool path correction has been reduced from the PV deviation of 9.59 to 3.60 waves. A quantitative analysis also is presented on the effects of misalignments and overlapping area of subapertures on stitching accuracy. The SHS has the potential to be incorporated into the machining platform during the freeform surface fabrication process; in addition, the feedback mechanism for the correction of the tool path demonstrated in this study can improve the surface profile accuracy efficiently. Further, the scheme is validated using coherence correlation interferometric optical profiler and the comparisons of the results are drawn.

References

[1] F. Duerr, Y. Meuret and H. Thienpont, Opt. Express 21, 31072–31081 (2013).
[2] F. Z. Fang, X. D. Zhang, A. Weckenmann, G. X. Zhang and C. Evans, CIRP Ann. Manuf. Technol. 62, 823–846 (2013).
[3] X. Zhang, L. Zheng, X. He, L. Wang, F. Zhang, et al., Proc. SPIE 8486 (2012).
[4] N. Takaki and P. R. Jannick, International Optical Design Conference, 10590 (International Society for Optics and Photonics, 2017).
[5] F. Kyle, P. R. Jannick and P. Th. Kevin, Opt. Express 19, 21919–21928 (2011).
[6] K. Ilhan, P. Th. Kevin and P. R. Jannick, Opt. Express 20, 22683–22691 (2012).
[7] S. Deepika, S. Kumar and R. G. Tilak, J. King Saud Univ. Comput. Inf. Sci. 29.1, 116–133 (2017).
[8] J. Philipp, M. Christoph and U. Karsten, Appl. Opt. 50, 822–828 (2011).
[9] C. Ozan, M. Brendan, F. Hassan and P. R. Jannick, Opt. Express 16, 1583–1589 (2008).
[10] P. Benitez, J. C. Miñano and M. Fernando, U.S. Patent No. 6,896,381 (2005).
[11] D. Ma, F. Zexin and L. Rongguang, Appl. Opt. 54, 498–503 (2015).
[12] E. Ruch, R. Geyl and H. Leplan, Optical Design and Fabrication 2017, OSA Technical Digest, JTh2B.6 (Freeform, IODC, OFT, 2017).
[13] H. Cai, J. Xu, J. Xiao, Y. Zhang and G. Shi, IOP Conf. Ser. Earth Environ. Sci. 69 (2017).
[14] K. Pang, F. Fengzhou, L. Song, Y. Zhang and H. Zhang, J. Opt. Soc. Am. B 34, B28–B35 (2017).
[15] W. B. Lee, H. Wang, S. To and C. F. Cheung, Mater. Sci. Forum 697 (2012).
[16] Z. Feng, B. D. Froese, R. Liang, D. Cheng and Y. Wang, Appl. Opt. 56, 9308–9314 (2017).
[17] S. A. Colburn, Z. Alan and M. Arka, CLEO: Applications and Technology, AW4O-4 (Optical Society of America, 2016).
[18] Y. Wang, Ch. Dewen and X. Chen, Freeform Optics, JTu3A-1 (Optical Society of America, 2017).
[19] D. Cheng, Y. Wang, H. Huaa and J. Sasian, Opt. Lett. 36, 2098–2100 (2011).
[20] H. Hong, H. Xinda and G. Chunyu, Opt. Express 21, 30993–30998 (2013).
[21] S. Stoebenau and S. Sinzinger, Proc. SPIE 7426 (2009).
[22] F. Niehaus, H. Stephan and G. Daniel, Int. Soc. Opt. Photon. 10448 (2017).
[23] V. Mishra, K. K. Pant, D. R. Burada, V. Karar, G. S. Khan, et al., Freeform Optics, FTh3B-2 (Optical Society of America, 2017).
[24] T. Blalock, M. Brunelle, I. Ferralli and B. Myer, International Optical Design Conference, JTh4B-1 (Optical Society of America, 2017).
[25] M. C. Knauer, J. Kaminski and G. Hausler, Proc. SPIE 5457, 366 (2004).
[26] H. Nouira, J. A. Salgado, N. El-Hayek, S. Ducourtieux, A. Delvallée, et al., Meas. Sci. Technol. 25, 044016 (2014).
[27] J. C. Wyant and K. N. Pretty Johns, Proc. SPIE 0661, 292 (1986).
[28] G. S. Khan, K. Mantel, I. Harder, N. Lindlein and J. Schwider, Appl. Opt. 46, 7040–7048 (2007).
[29] G. S. Khan, M. Bichra, A. Grewe, N. Sabitov, K. Mantel, et al., 3rd EOS Conference on Manufacturing of Optical Components, 13–15 (2013).
[30] S. Sebastian, B. Matthias, Z. Uwe-Detlef, R. Stefan and G. Andreas, Proc. SPIE 8613 (2013).
[31] P. Murphy, G. Forbes, J. Fleig, P. Dumas and M. Tricard, Opt. Photon. News 14, 38–43 (2003).
[32] G. Baer, J. Schindler, C. Pruss, J. Siepmann and W. Osten, Int. J. Optomech. 8, 242–250 (2014).
[33] A. Beutler, Surf. Topogr. Metrol. Prop. 4, 024011 (2016).
[34] G. Berger and W. Marc. Opt. Photon. 13.1, 40–43 (2018).
[35] J. Yao, A. Anderson and J. P. Rolland, Opt. Express 26, 10242–10265 (2018).
[36] K. K. Pant, D. R. Burada, M. Bichra, M. P. Singh, A. Ghosh, et al., Appl. Opt. 54, 10022–10028 (2015).
[37] D. R. Burada, K. K. Pant, M. Bichra, G. S. Khan, S. Sinzinger, et al., Opt. Eng. 56, 084107 (2017).
[38] K. K. Pant, D. R. Burada, M. Bichra, A. Ghosh, G. S. Khan, et al., Appl. Opt. 57, 1100–1109 (2018).

[39] D. R. Burada, K. K. Pant, V. Mishra, M. Bichra, G. S. Khan, et al., Proc. SPIE 10329 (2017).
[40] N. Lindlein, F. Simon and J. Schwider, Opt. Eng. 37, 1809–1816 (1998).

Dali Ramu Burada
Instrument Design Development Centre, Indian Institute of Technology Delhi, New Delhi 110016, India

Dali Ramu Burada is a research scholar at the Indian Institute of Technology (IIT) Delhi. He received his M.Tech. in applied optics from the IIT Delhi in 2012. He is working in the field of optical metrology since 2012. His area of interest is metrology of nonconventional optical surfaces such as freeform optics for imaging and nonimaging applications.

Kamal K. Pant
Instrument Design Development Centre, Indian Institute of Technology Delhi, New Delhi 110016, India; and Instruments Research and Development Establishment, Dehradun 248008, India

Kamal K. Pant is a research scholar at the IIT Delhi. He received his M.Tech. in applied optics from the IIT Delhi in 2010. Currently, he is working as a scientist in IRDE Dehradun. His research interests are development of freeform optics and diffractive optics for imaging applications, subaperture stitching-based metrology of freeform optics, and SHS-based metrology.

Vinod Mishra
Instrument Design Development Centre, Indian Institute of Technology Delhi, New Delhi 110016, India; and CSIR-Central Scientific Instruments Organisation, Chandigarh 160030, India

Vinod Mishra is a technical officer at CSIR-CSIO Chandigarh. He finished his Master's in mechanical engineering and pursuing Ph.D. at the IIT Delhi. His area of research is ultra-precision machining, surface finishing, optics fabrication, and metrology. He has more than 10 years of research and development experience in ultra-precision machining. He has more than 20 publications including various international and national journals and conference proceedings.

Mohamed Bichra
Fachgebiet Technische Optik, Technische Universität Ilmenau, 98693 Ilmenau, Germany

Mohamed Bichra studied micro and medical technology with a particular focus on laser systems at the University of Applied Sciences Gelsenkirchen. In 2009, he graduated with an engineering degree from the same university. Between 2008 and 2012, he has worked as a development engineer at Limo Lissotschenko Mikrooptik GmbH in Dortmund and at Heinz Group in Elgersburg. Since 2012, he is a Ph.D. student and research assistant with Prof. Sinzinger at Technische Universität Ilmenau.

Gufran Sayeed Khan
Instrument Design Development Centre, Indian Institute of Technology Delhi, New Delhi 110016, India
gufranskhan@iddc.iitd.ac.in.
https://orcid.org/0000-0001-7911-565X

Gufran Sayeed Khan is an associate professor at the Instrument Design Development Centre, IIT Delhi. He received his Ph.D. in optical engineering from the International Max Planck Research School at University of Erlangen-Nuremberg, Germany. He was a NASA postdoctoral fellow at the Marshall Space Flight Centre, Huntsville, AL, USA. His research interest is in optical metrology with a particular focus on the development of diffractive, aspheric, and freeform optics for imaging and nonimaging application.

Stefan Sinzinger
Fachgebiet Technische Optik, Technische Universität Ilmenau, 98693 Ilmenau, Germany

Stefan Sinzinger received his diploma in physics and Ph.D. from the Friedrich-Alexander Universität Erlangen Nürnberg, Institute for Applied Optics (Professor Dr. A.W. Lohmann) in 1989 and 1993, respectively. In 2002, he became a professor of optical engineering (Technische Optik) at the Technische Universität Ilmenau. He has more than 190 publications in international journals and conferences. He is a coauthor of the textbook *Microoptics* and editor of the textbook *Optical Information Processing* (author: A.W. Lohmann). His current research focuses on the design, integration, fabrication, and application of (micro)optical elements and hybrid optical (micro)systems.

Chandra Shakher
Instrument Design Development Centre, Indian Institute of Technology Delhi, New Delhi 110016, India

Chandra Shakher is an Emeritus professor at the Instrument Design Development Centre, IIT Delhi. He received his Ph.D. from the IIT Madras in 1980. His research interest includes holography interferometry, speckle metrology, fiber optic current sensors, optical coherence tomography, and laser-based instrumentation. He has more than 100 publications in international journals and more than 75 in conference proceedings. He is the recipient of the ICO Galileo Galilei Award of 2014. He is a fellow SPIE, OSA, Indian National Academy of Engineering.